Electroaddressing Functionalized Polysaccharides as Model Biofilms for Interrogating Cell Signaling

*Yi Cheng, Chen-Yu Tsao, Hsuan-Chen Wu, Xiaolong Luo, Jessica L. Terrell, Jordan Betz, Gregory F. Payne, William E. Bentley, and Gary W. Rubloff**

Bacteria often reside at surfaces as complex biofilms in which an exopolysaccharide matrix entraps the population while allowing access to its chemical environment. There is a growing awareness that the biofilm structure and activity are integral to a wide array of properties important to health (the microbiome), disease (drug resistance) and technology (fouling). Despite the importance of bacterial biofilms, few experimental platforms and systems are available to assemble complex populations and monitor their activities. Here, a functionalized alginate composite material for creating in vitro model biofilms suitable for cell-cell signaling studies by entrapping bacterial cells in situ is reported. Biofilm assembly is achieved using device-imposed electrical signals to electrodeposit the stimuli-responsive polysaccharide alginate. This electrodeposition mechanism is versatile in that it allows control of the bacterial population density and distribution. For instance, it is demonstrated that a mixed population can be homogeneously distributed throughout the biofilm or can be assembled as spatially segregated populations within a stratified biofilm. The "electroaddressable" biofilms are visualized using both a planar 2D chip with patterned electrodes and a microfluidic bioMEMS device with sidewall electrodes. Specifically, it is observed that bacteria entrapped within the model biofilm recognize and respond to chemical stimuli imposed from the fluidic environment. Finally, reporter cells are used to demonstrate that bacteria entrapped within this model biofilm engage in intercellular quorum sensing. This work demonstrates the functionality of the stimuli-responsive polysaccharide by biofabricating pseudo-3D cell-gel biocomposites, mimicking the formation of biofilms, for interrogating phenotypes of *E. coli* bacterial populations. In addition to controlling assembly, the microfluidic device allows the biofilm to be monitored through the fluorescence methods commonly used in biological research. This platform technology should be able to be exploited for monitoring biofilm development, as well as for extending the understanding of the interactions between various bacterial species arranged in controlled patterns.

1. Introduction

Pathogenic bacteria and the problems they create are on the rise, exemplified by the emergence of antibiotic-resistant "superbacteria"[1–3] and the recalcitrance of bacterial biofilms[4–6] that are exposed to antibiotic treatments. Antimicrobial research strategies are emerging that target the cell-cell communication networks,[7,8] in contrast to directly attacking and killing the bacteria, which has the associated risk of encouraging antibiotic resistance in the surviving population. There exists a great need for new experimental platforms[9] that facilitate the study of bacterial cells with the capability of spatially localizing them in a multidimensional microenvironment,[10] as well as probing the cell physiology, communication and population-scale behaviors of the assembled bacterial populations at a system level.

3D structures of natural or synthetic polymer materials are suitable for this task[11–13] because of their unique structural and mechanical properties and their stability, both chemically and physically, providing physiologically relevant cellular microenvironments.[14–20] Polysaccharides, a category of natural polymeric carbohydrate structures, are ideal candidates for this purpose. In particular, the polysaccharide, alginate, shares the same composition as the extracellular polymeric substance (EPS) secreted by bacteria.[21,22] This suggests significant advantages in using these materials to fabricate a bottom-up

Dr. Y. Cheng, J. Betz, Prof. G. W. Rubloff
Institute for Systems Research
University of Maryland
College Park, MD 20742, USA
E-mail: rubloff@umd.edu
Dr. C.-Y. Tsao, H.-C. Wu, Dr. X. Luo, J. L. Terrell, Prof. G. F. Payne, Prof. W. E. Bentley
Institute for Bioscience and Biotechnology Research (IBBR)
University of Maryland
College Park, MD 20742, USA
Dr. C.-Y. Tsao, H.-C. Wu, J. L. Terrell, J. Betz, Prof. G. F. Payne, Prof. W. E. Bentley
Fischell Department of Bioengineering
University of Maryland
College Park, MD 20742, USA
Prof. G. W. Rubloff
Department of Materials Science and Engineering
University of Maryland
College Park, MD 20742, USA

DOI: 10.1002/adfm.201101963

hydrogel matrix that entraps cells and provides a viable environment for continued cell growth.

The fact that gelation of charged polysaccharides can be induced by an electrical signal[23,24] enables us to construct customized model biofilms with controllable size, thickness and location and tunable cell composition. Specifically, electroinduced gelation of stimuli-responsive polysaccharides[25–28] relies on localized electrical signals that generate gradients of crosslinker species (Ca^{2+} ions) electrochemically on the electrode surface.[29] This enables spatial selectivity and addressability of soft materials within device environments constructed by solid-state-device microfabrication.[23,30]

While our group and others have demonstrated polysaccharide electroaddressing,[23–28,31] several challenges remain for in situ cell-gel assembly: i) retaining full biological activity during and after the localized electrochemical reactions that trigger the sol-gel transition; ii) developing methods to selectively address different cell populations at specific locations with lateral spatial control; and iii) enabling the properties of the hydrogel scaffold to facilitate the study of cellular and intercellular processes.

Here, we present a functionalization process to assemble an alginate composite that is capable of localizing bacterial cells within its gel structure onto conductive surfaces for cell-signaling studies. This "biofabrication" process, which mimics natural processes and exploits biological components, is realized by entrapping bacterial colonies in situ using a stimuli-responsive polysaccharide whose gelling process can be triggered and controlled by electrical signals under physiological conditions.

Firstly, the electroaddressing capability is demonstrated by co-depositing *Escherichia coli* (*E. coli*) cells with a calcium alginate gel in a programmable, electrode-templated pattern using planar microfabricated chips. Several strains of the *E. coli* populations are electroassembled and spatially confined onto 2D, prepatterned electrode surfaces in an array format with desired addresses. Secondly, *E. coli* cell assembly is quantitatively electroaddressable in pseudo-3D model biofilms as visualized via a transparent fluidic device with sidewall electrodes. The same device is used to demonstrate simultaneous multistrain assembly in stratified and segregated patterns where spatial control in the third dimension (perpendicular to the electrode plane) is presented by device-generated signals. The exogenous addition of small molecules (isopropyl β-d-1-thiogalactopyranoside (IPTG)) and the endogenous generation of cell-cell signaling molecules mediate the controlled cell phenotype within the microfluidic device. The approach is enabled with a highly functional platform to study signaling among different cell populations in the microfluidic device. This platform may prove useful for spatially evaluating the role of quorum-sensing autoinducer molecules responsible for organized multicellularity, a phenomenon contributing to complex biofilm behaviors.

2. Results and Discussion

2.1. Electrodeposition of the Calcium Alginate Hydrogel

2.1.1. The Microfluidic Device and the Electrodeposition of Calcium Alginate

Initial evidence for the electrodeposition of calcium alginate hydrogel was provided by experiments with the fluidic device that is illustrated in **Figure 1**a–d. The fabrication procedure of the fluidic device has been reported previously.[29] Briefly, this device was fabricated with multiple paired electrodes defined on the two sidewalls of the fluidic channel. The transparent polydimethylsiloxane (PDMS) layers covering the top and bottom of the channel allowed the dimensional profile of the electrodeposited hydrogel and subsequent fluorescent signals to be observed.

The electrodeposition procedure can be divided into three steps: firstly, the fluidic channel was filled with the alginate solution, which contained suspended $CaCO_3$ particles. Secondly, a constant current density of 4 A m^{-2} was applied on one sidewall electrode for a certain period of time (typically 1–2 min), with the opposite electrode grounded. The mechanism of the anodic electrodeposition of calcium alginate was reported recently.[24] Briefly, water electrolysis on the anode surface electrochemically generates protons that react with the suspended $CaCO_3$ particles and locally release Ca^{2+} ions. The Ca^{2+} ions then crosslink the alginate polymer chain and form the hydrogel. Thirdly, to remove any non-deposited alginate and $CaCO_3$ particles after deposition, the channel was evacuated and then rinsed with 10×10^{-3} M sodium chloride (NaCl) solution. Detailed discussion of the mechanism is provided in the supporting information (Figure S1, Supporting Information). The results from this experiment are shown in Figure 1b–d. A semioval-shaped, cloudy-white deposited material was observed on the anodic sidewall electrode via the side view of the fluidic device (Figure 1b). In the top view of the device, with the transmitted light coming from below, the hydrogel appeared opaque in color as the insoluble $CaCO_3$ particles blocked the light transmission (Figure 1c).

2.1.2. Physical Evidence of the Electrodeposition

Independent evidence for the electrodeposition of calcium alginate hydrogel was provided by optical and fluorescence microscopy. To observe and record the alginate-hydrogel electrodeposition, an upright optical microscope equipped with a charge-coupled-device (CCD) camera was used to focus on the electrodes within the channel. To aid the visualization, we used amine-modified fluorescent microspheres (1 μm diameter) to fluorescently label the alginate through amine-carboxylate interactions. The same deposition procedure was repeated and the device was then examined using both optical microscopy (with the transmitted light coming from below) and fluorescence microscopy. Results from this experiment are shown in Figure 1e–g. Figure 1e, on the top row, shows the bright-field image and Figure 1e', on the bottom row, shows the fluorescence images. The fact that the size and shape of the gel are consistent in each bright-field image and corresponding fluorescence image suggests a successful deposition of alginate with entrapped $CaCO_3$ particles. In Figure 1e', a uniform distribution of the fluorescence is observed within the hydrogel, which suggests a uniform density of the cross-linked alginate polymer chains. The hydrogel was then detached from the electrodes by excessive flow stress and placed on a glass slide for imaging. The detached hydrogel remained intact as a whole piece on the glass slide and exhibited a relatively uniform distribution of $CaCO_3$ particles (Figure 1f and 1g) and cross-linked alginate polymer chains (Figure 1f' and 1g').

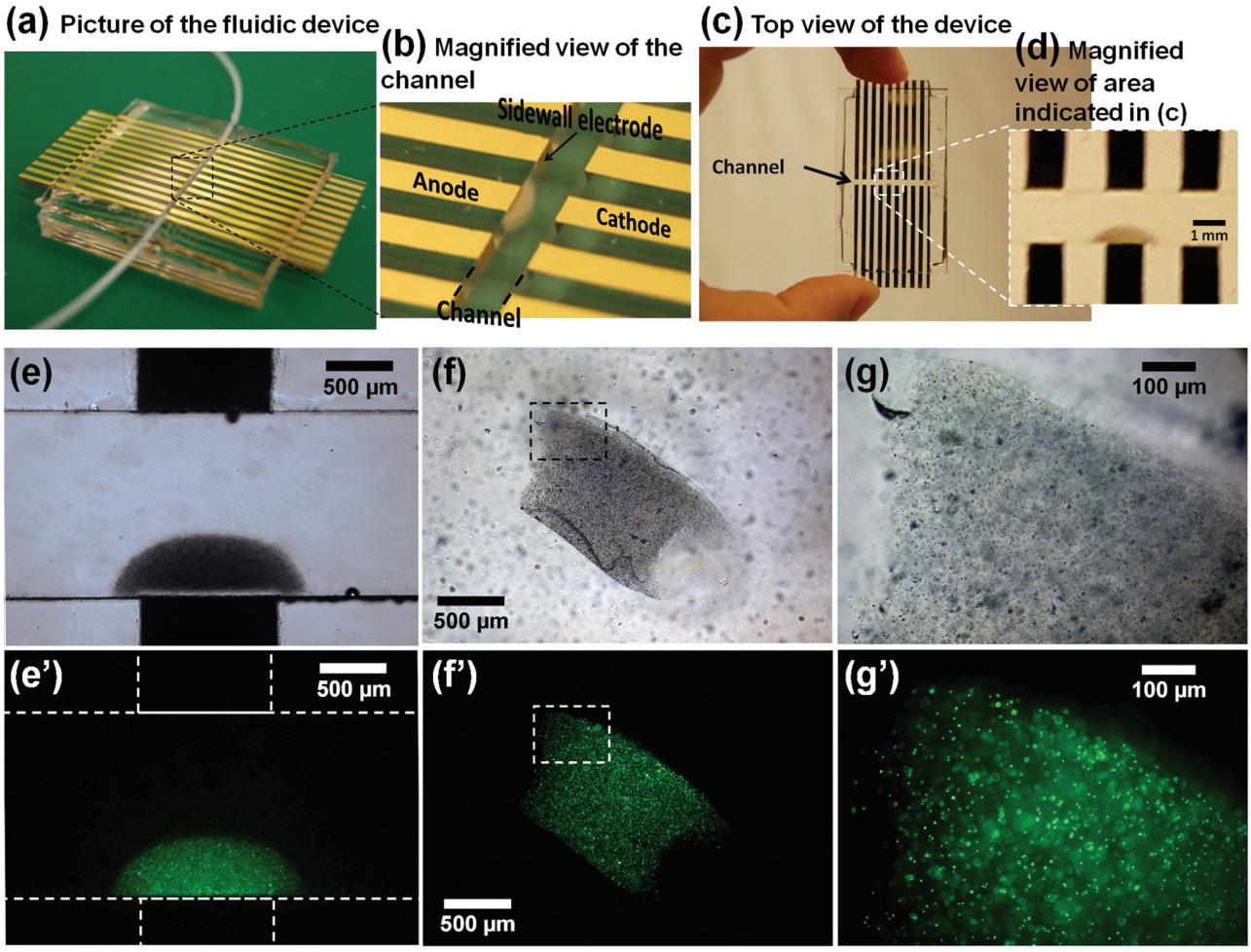

Figure 1. Pictures of the fluidic device and micrographs of the electrodeposited calcium alginate hydrogel. a) An overview of the fluidic device with built-in sidewall electrodes inside the channel and plastic tubes connected as an inlet and outlet. b) A magnified view of the fluidic device with a cloudy-white hydrogel deposited on one of the sidewall electrodes (anode). c) Top view of the fluidic device. d) A magnified top view of the fluidic channel with the electrodeposited hydrogel on one of the electrodes. e–e′) Optical (e) and fluorescence (e′) micrographs of a calcium alginate hydrogel (side view) deposited on an anodic electrode inside the fluidic channel. f–f′) Optical (f) and fluorescence (f′) micrographs of the calcium alginate hydrogel (top view) detached from the electrode and placed on a glass slide. g–g′) Magnified optical (g) and fluorescence (g′) micrographs of a part of the hydrogel.

Additionally, compositional analysis of the deposited materials by Raman spectroscopy confirmed that the electrodeposited material contained calcium alginate and insoluble $CaCO_3$. Detailed results and discussion are given in the supporting information (Figure S2, Supporting Information).

2.2. *E. coli* Cell Assembly with the Co-deposition of Calcium Alginate Gel

2.2.1. Spatiotemporally Controllable Cell Assembly

One of the important applications of alginate hydrogels is cell immobilization.[32,33] Since the alginate abundantly exists in the matrix of extracellular polymeric substances (EPS) in the biofilm produced by bacterial cells,[21,22] our ability to assemble it controllably in a microfluidic environment enables it to serve as a model material, forming a cohesive polymer network that interconnects and immobilizes bacterial biofilm cells. The spatiotemporal, programmable cell assembly with electrodeposition of calcium alginate on 2D surfaces was firstly examined on arrayed and arbitrary electrode patterns.

Cells were firstly suspended in an aqueous deposition solution that contained alginate and suspended $CaCO_3$ particles. Their entrapment on an individual electrode was achieved by localized gelation of alginate triggered by the electrochemically released calcium ions. Subsequent evacuation of the deposition solution and rinsing with NaCl were performed to remove the uncrosslinked alginate and nonentrapped cells. The consistently high viability of *E. coli* before and after encapsulation was demonstrated (Figure S7, Supporting Information).

To demonstrate the assembly of a bacterial-cell array, we designed a pattern with a 5 × 5 array of electrodes, shown in **Figure 2**a. Here, each circular electrode was independently

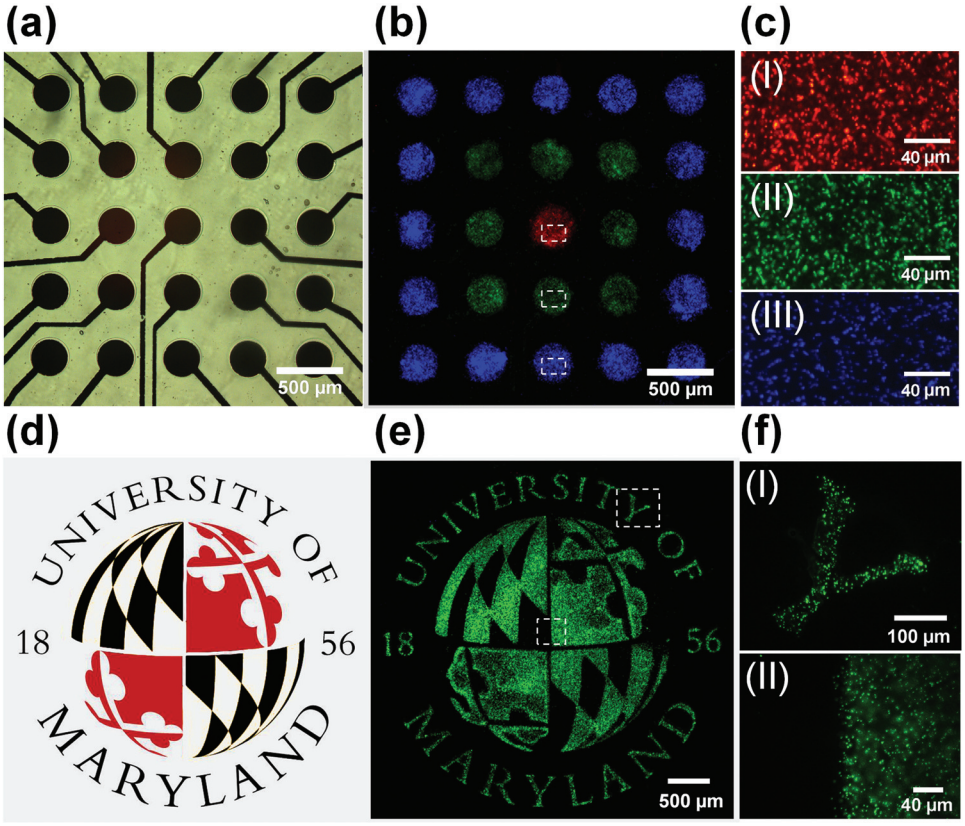

Figure 2. Multistrain, multiaddress cell assembly in array format and monostrain cell assembly on an arbitrary pattern. a) Optical micrograph with transmitted light from below showing the 5 × 5 circular electrode array. Each electrode was connected independently to one contact pad through a contact lead. The contact leads were passivated with SiO_2. b) Fluorescence micrograph of an assembled array of cells with red, green and blue fluorescent protein expression. c) Magnified views of the red (I), green (II), and blue (III) fluorescent protein expressing the *E. coli* cells assembled on the individual electrodes. The zoomed-in regions are marked with the white dashed rectangles in Figure 2b. d) The logo of the University of Maryland: the logo was printed out on a transparency as a photomask to pattern the electrode. e) Fluorescence micrograph showing that the pattern of the logo consisted of assembled *E. coli* cells expressing GFP, which were entrapped by the co-deposition with calcium alginate. f) Magnified view of the letter Y (I) in the upper right of the logo and the edge between the patterned region and unpatterned region with and without assembled cells (II).

addressed by its connection to one contact pad (not shown in Figure 2a). The electrode contact leads were passivated with insulating SiO_2 to prevent leakage conduction from the leads. The cell assembly could be easily scaled up to an array of electrode addresses by simultaneously applying current on multiple electrodes with proportionally increased electric current. In this way, multisite assembly could be achieved in a single deposition run. One can also apply a current on selective electrode addresses to create specific patterns within the 5 × 5 array.

To facilitate visualization, we used *E. coli* BL21(DE3) bearing different plasmids (pET-DsRed, pET-GFP and pRSET/BFP) to express different fluorescent proteins.[34] Here DsRed is a kind of red fluorescent protein (RFP), while GFP and BFP stand for, analogously, "green fluorescent protein" and "blue fluorescent protein". These cells will be referred to in short as red, green and blue *E. coli* cells, respectively. To demonstrate cell assembly in an array format, the red, green and blue *E. coli* cells were separately blended into three deposition solutions and sequentially assembled on a patterned 5 × 5 array of electrodes to demonstrate a dot-and-square-shaped pattern. Figure 2b shows a fluorescence micrograph taken after sequential electrodepositions (4 A m^{-2} for 60 s) of the red, green and blue fluorescent cells (optical density (OD) = 3) selectively on the desired electrode addresses. Figure 2c(I–III) shows the magnified fluorescence micrograph of the cells entrapped on the electrodes. The results demonstrate that the cell assembly with calcium alginate electrodeposition was spatially confinable and address-programmable.

To further demonstrate the electroaddressing capability and to estimate the spatial resolution of this assembly method, we fabricated a planar electrode pattern of the University of Maryland (UMD) logo. The original logo, shown in Figure 2d, was used as a photomask to pattern the electrode. With alginate serving as an electrotemplated coupling between the cells and the electrode, cell assembly onto specific locations in an arbitrary pattern could be easily achieved with micropatterning. A deposition solution containing GFP-expressing *E. coli* cells (OD = 3) was added dropwise onto the electrode and deposition was carried out at 4 A m^{-2} for 30 s. The deposition solution was then removed and the electrode was rinsed with NaCl solution before imaging. Figure 2e shows the fluorescence

micrograph of the logo pattern with assembled green *E. coli* cells. Figure 2f(I–II) shows magnified fluorescence images of the letter "Y" and the edge between the cell-assembled region and cell-free region, as marked in Figure 2e. The results demonstrate that our cell assembly was highly controllable and a lateral resolution down to tens of micrometers could be achieved.

2.2.2. Quantitative Cell Assembly by Tuning the Cell Density and Deposition Time

Bacterial biofilms grow at very slow rates and tend to maintain a high cell density in the EPS matrix, which makes them resistant to chemical stress, such as that imposed by antibiotics and chlorine-based disinfection. The capability of controlling the cell density in the rapidly formed alginate hydrogel is attractive for addressing population-based or density-dependent phenomena of the communal form of cellular organization within a model biofilm, such as in antibiotic-resistance development[35,36] and cell-cell signaling networks studies.[37] In this section, we demonstrate that the *E. coli* assembly with electrodeposition of alginate could be quantitatively controlled. Specifically, the final cell number in the alginate hydrogel was tunable by: i) varying the initial cell density in the deposition solution, and ii) controlling the electrodeposition time, which, in turn, determines the gel volume/thickness.

To aid visualization, here we used *E. coli* BL21(DE3) bearing plasmid (pET-DsRed) to express the red fluorescent protein (DsRed). The cells were initially cultured in Luria–Bertani (LB) medium overnight to an optical density (OD_{600}) of 3.0 and then concentrated to OD_{600} = 12 by centrifugation and resuspension. A series of dilutions was performed to obtain cell solutions with decreasing concentrations, as measured by OD_{600}. By controlling the cell concentration mixed with alginate solution (2% alginate, 0.5% $CaCO_3$), quantitative control of the cell assembly could be realized by electrodepositing alginate hydrogels for an equivalent amount of time. **Figure 3**a(I–VI) shows the results from electrodeposited alginate hydrogels with increasing concentrations (OD = 0.6, 1.2, 3, 6, 9, and 12) of entrapped seeding cells. The current density was 5 A m^{-2} and the deposition time was 65 s. As shown in Figure 3b, the integrated fluorescence intensities of the gel regions show a linear dependence on the cell density blended in the deposition solution. The number of entrapped cells could also be controlled by the electrodeposition time. Figure 3c(I–VI) shows the results of cell assembly after varying the electrodeposition time (30, 45, 60, 75, 90, 130 s) at 5 A m^{-2} using a deposition solution containing a constant cell density (OD = 4). As shown in Figure 3d, the integrated fluorescence intensity of the gel region exhibited a linear dependence on the deposition time. These results demonstrate that quantitative co-deposition and controllable entrapment of cell populations within calcium alginate gels could be realized.

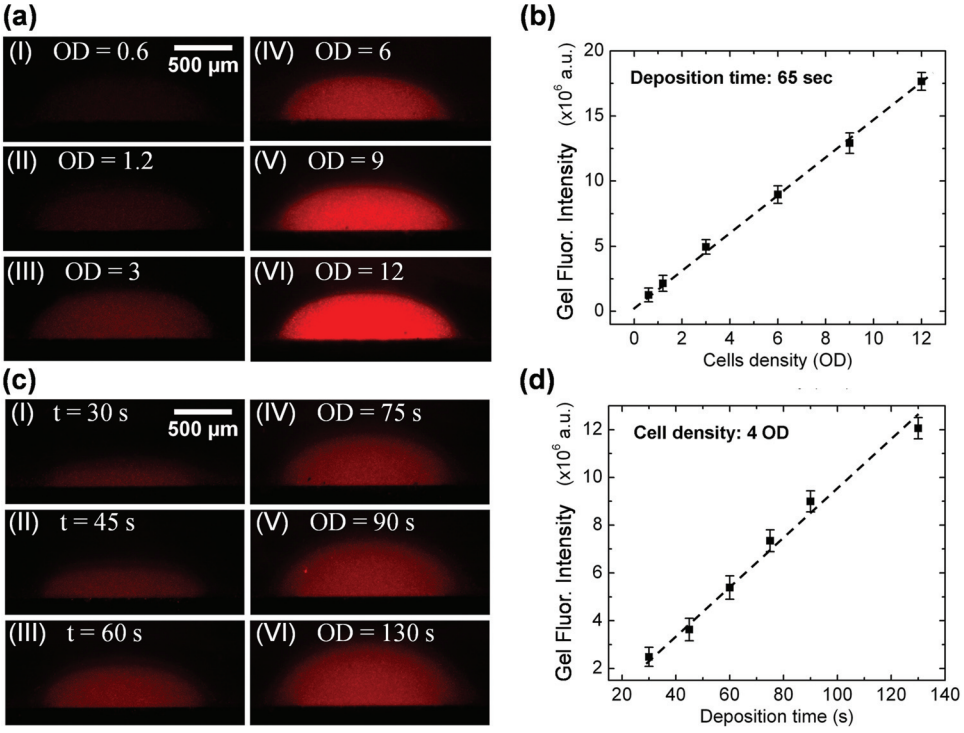

Figure 3. Quantitative assembly of *E. coli* cell populations on an individual electrode. a) I–VI are a series of fluorescence micrographs of entrapped RFP-expressing *E coli* cells after 65 s of gel electrodeposition at 5 A m^{-2} by mixing different concentrations of cells (optical density: 0.6, 1.2, 3, 6, 9 and 12) with the alginate solution (2% alginate, 0.5% $CaCO_3$). b) Plot of the integrated fluorescence intensity of the gels shown in Figure 3a(I–VI) as a function of cell density. c) I–VI are a series of fluorescence micrographs of entrapped RFP-expressing *E coli* cells in the electrodeposited alginate gel using different deposition times (30, 45, 60, 75, 90 and 130 s) with a fixed cell density (OD = 4) of the deposition solution and identical current densities. d) Plot of the integrated fluorescence intensity of the gels shown in Figure 3c(I–VI) as a function of deposition time.

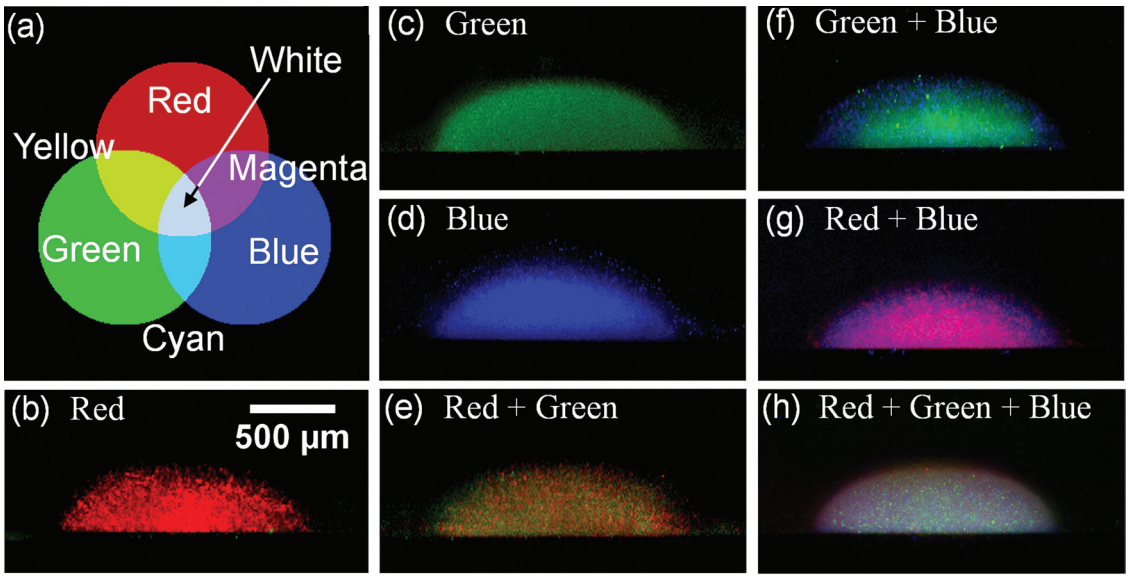

Figure 4. Monostrain and multistrain cell assembly. a) A schematic representation of additive color mixing. The combination of any two or three primary colors (red, green and blue) makes secondary colors (yellow, cyan, magenta and white). b–h) Monostrain cell assembly of red (b), green (c), and BFP-expressing (d) *E. coli* cells and multistrain cell assembly of red + green (e), green + blue (f), red + blue (g) and red + green + blue (h) fluorescent-protein-expressing *E. coli* cells entrapped in the electrodeposited alginate gels.

2.2.3. Multistrain Cell Coassembly with a Pseudo-3D Hydrogel

Bacterial biofilms are integrated, multispecies communities of cells with complex and diverse formats. A recent study revealed that they are co-ordinated and co-operative groups, analogous to multicellular organisms.[38] Our cell-assembly approach can be easily applied to the simultaneous assembly of heterogeneous populations of bacteria in one-step electrodeposition, mimicking the multispecies bacterial organization of biofilms.

In this section, we demonstrate multitype cell assembly by simultaneous co-deposition. To aid the visualization, we again used the red, green and blue *E. coli* cells. We prepared deposition solutions containing one, two and three types of *E. coli* cells. Multiple electrodepositions were performed under the same conditions (current density = 5 A m^{-2}, deposition time = 70 s). The deposited cell populations were examined using TRITC, GFP, and BFP filter sets. Superimposed images taken using the individual filters were merged to show all of the cell populations entrapped inside. **Figure 4** shows a combinatorial experiment with seven independent depositions of red (R), green (G), blue (B), R + G, R + B, G + B and R + G + B *E. coli* cell populations. A broad spectrum of colors was produced, in addition to the primary R, G and B colors due to the combined expression of multiple colors of proteins by cohabiting cell populations. The relative intensity of one or two cell populations in the deposited hydrogel could be varied by tuning the initial mixing density of the desired cell population(s).

Since the calcium alginate gelation was reversible and the gel could be disassembled using sodium citrate, the entrapped cells could be released for further analysis. The disassembly of the gel and the release of the entrapped green *E. coli* with sodium citrate solution (Figure S3, Supporting Information) and the consistently high viability of *E. coli* before and after gel dissolution (Figure S7, Supporting Information) were demonstrated.

These results confirm that different strains of cells not only can be assembled sequentially onto different electrode addresses with controlled separation, but also can be assembled simultaneously with immediate adjacency in a single layer of model biofilm. This is a valuable functionality for studying the cellular behavior of one type in response to the presence of the other, or the interactions between different cell species during coculture in close contact. Furthermore, additional analysis can be performed on individual cells after disassembling the gel and collecting the released cells downstream.

2.2.4. Stratified and Segregated Cell Assembly with Controlled Separation

So far, we have demonstrated 2D spatial control over the location, the number of species and the quantity of the cell populations assembled in the model biofilms. In reality, biofilms are highly structured and often adopt a 3D configuration with spatial heterogeneities. In this section, the capability of our approach of controlling cell assembly over the third dimension is demonstrated. Specifically, we demonstrate our results by sequentially assembling different cell strains in multilayer calcium alginate gels with an adjustable distance between the layers.

We sequentially deposited multiple cell populations on one electrode. **Figure 5**a–d demonstrates a separable, multilayer cell immobilization by sequentially using deposition solutions with and without green fluorescent *E. coli*. Clearly, green fluorescent *E. coli* could be entrapped into selected layers of the hydrogel with a controllable separation, and thus different cell populations could also be assembled in the immediate vicinity of each other. Figure 5e–f shows the multilayer immobilization of red,

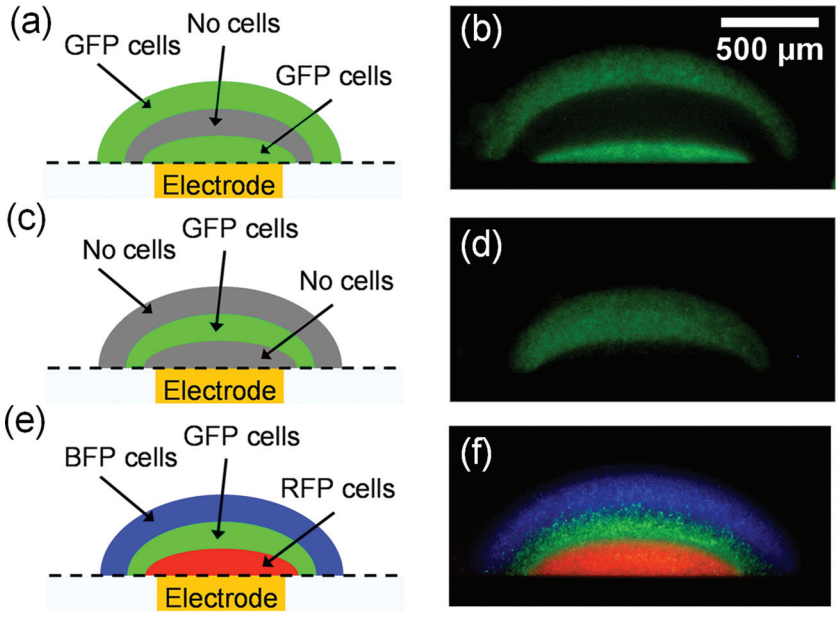

Figure 5. Multilayer cell assembly on individual electrodes. a–b) Schematic diagram (a) and fluorescence micrograph (b) of a multilayer structure of, sequentially, an electrodeposited alginate gel with a layer of pure gel sandwiched by two layers of gel with entrapped *E. coli* cells expressing GFP. c–d) Schematic diagram (c) and fluorescence micrograph (d) of a multilayer structure of sequentially electrodeposited alginate gels with a layer of gel with entrapped *E. coli* cells expressing GFP sandwiched by two layers of pure alginate gel. e–f) Schematic diagram (e) and fluorescence (f) micrograph of a multilayer structure of cell populations with a co-deposition sequence of RFP-, GFP- and BFP-expressing *E. coli* cells.

green and blue fluorescent *E. coli* populations by sequentially depositing alginate gels that contained red, green and blue *E. coli*, respectively.

The ability of flexibly creating multilayer model biofilms of stratified and segregated bacterial populations with well-defined spatial extents such that the spatial localization of the different cell types with respect to each other is controlled is an attractive feature in understanding the distance-dependent communication and interactions between cell colonies of the same or different types under different microenvironments. Additionally, such a spatially heterogeneous cell-gel production with tunable gel properties and definable cell locations could be useful in studying the permeation and diffusion of nutrients and oxygen, the transport of intercellular signaling molecules and the interfacial properties between different bacterial colonies by creating layered structures with different accessibilities to extracellular chemical concentrations.

2.3. In-Gel Cell Functions: Induced Protein Expression and Quorum Sensing in *E. Coli* Cells in Electrodeposited Hydrogels

2.3.1. In-Gel-Induced Protein Expression

To examine whether entrapped cells in an electrodeposited model biofilm can respond to the stimuli of the external environment, we used recombinant *E. coli* that expressed fluorescent proteins in response to a chemical inducer. In particular, we used recombinant *E. coli* (BL21(DE3) bearing pET-RSET/BFP plasmid) that can express BFPs by IPTG induction.

Initially, the cells were co-deposited with alginate and $CaCO_3$, and cells within the gel exhibited no BFP expression, as shown in the optical micrograph (**Figure 6**a) and fluorescence micrograph (Figure 6b). After thorough rinsing with NaCl, a culturing solution (LB medium with 10×10^{-3} M $CaCl_2$) was injected in the channel to maintain the structural integrity of the gel and provide nutrients to the cells. IPTG was then introduced into the culturing solution (final concentration: 1×10^{-3} M), which flowed through the fluidic channel housing the gel-entrapped cells at a constant flow rate of 5 μl min^{-1}. During the whole process, the fluidic device was kept in an incubator at 37 °C. The fluorescence of the gel was recorded every 4 h. Figure 6d shows the fluorescence intensity of the gel as a function of induction time (or hour post-induction). Here the values were derived from image analysis of the fluorescence intensities integrated over the gel region. The fluorescence intensity of the gel increased linearly during the 12 h of incubation. The fluorescence of the negative-control cells that had been co-deposited but not induced by IPTG showed nearly no change along the time course. Figure 6c shows a fluorescence micrograph of the gel after 12 h of incubation. The bright blue color within the gel region confirms active BFP was expressed by the entrapped cells in response to external chemical stimuli.

2.3.2. In-Gel Bacterial Quorum Sensing

Finally, we examined the communication between different strains of *E. coli*, known as bacterial quorum sensing.[37,39–41] Bacteria can communicate with each other with a small, and self-generated signaling molecule called autoinducer 2 (AI-2). The cells not only synthesize and secrete AI-2, but they also sense AI-2 in their environment, as produced by the same or different species, to trigger changes in their gene expression and cell phenotype. Understanding and ultimately interfering with the AI-2-mediated bacterial communication could lead to therapeutic strategies for preventing the transition from single-cell behavior to co-ordinated multicelluar behavior, such as biofilm formation.[42] Quorum sensing is a population-based and concentration-dependent phenomenon. Autoinducer secreted from low-cell-density populations is benign. However, as the population grows, autoinducer concentrations rise and reach a threshold at which the quorum-sensing regulated genes are activated. With the capability of forming pesudo-3D gels and with the sidewall-electrode-enabled microfluidic-device platform, our biofabrication-based assembly strategy provided an ideal tool for this study.

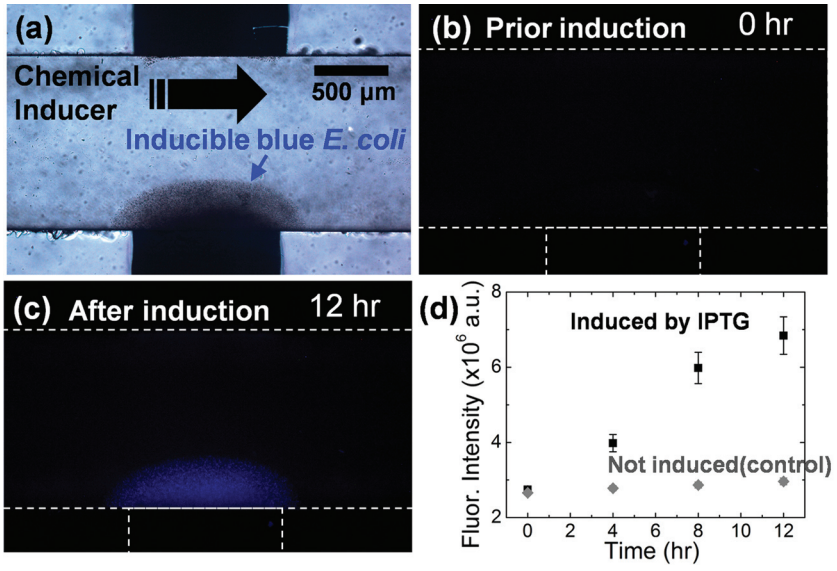

Figure 6. Induction of entrapped *E. coli* cells to promote BFP expression. a) Bright-field optical image showing the co-deposition of BL21 (pET-BFP) with calcium alginate. b) Flurorescence image of the gel with entrapped cells before induction. c) Fluorescence image of the gel with induced cells after 12 h induction. d) Time course of the fluorescence intensity of the gel. The grey dots represent a control sample without introducing the chemical inducer, IPTG.

We employed two types of *E. coli* strains: reporter cells and transmitting cells. The reporter cell, MDAI2 (pCT6 + pET-DsRed), was the AI-2 synthase, *luxS,* knock-out strain, which cannot produce AI-2 but can sense the AI-2 signaling molecule to trigger the expression of DsRed.[34] The transmitting cells, BL21 (pCT5 + pET-GFP$_{uv}$), can constitutively express GFP and produce the signaling molecule AI-2.

We firstly co-deposited MDAI2 (pCT6 + pET-DsRed) reporter cells (OD = 3) and the calcium alginate gel in the fluidic channel. An optical micrograph of the channel with entrapped cells in the deposited gel is shown in **Figure 7**a. The culturing solution containing BL21 (pCT5 + pET-GFP$_{UV}$) transmitting cells (OD = 6), $CaCl_2$ (10×10^{-3} M) and LB medium was flowed into the channel and recirculated throughout the channel. A fluorescence micrograph of the channel using a GFP filter set is shown in Figure 7c. The BL21 (pCT5 + pET-GFP) transmitting cells stayed in the liquid phase, producing and secreting the signaling molecule AI-2. The reporter cells entrapped in the gel at the electrode should respond to AI-2 and express DsRed.

The co-cultures were incubated at 37 °C for 20 h. The fluorescence micrographs taken at 0 and 20 h in Figure 7d and Figure 7e show a dramatic increase in red fluorescence of the entrapped reporter cells. To demonstrate that the increase in fluorescence was due to the presence of the signal-production cells, we applied the negative control, coculturing with the same concentration of entrapped MDAI2 reporter cells in the liquid phase (with only $CaCl_2$ (10×10^{-3} M) and LB medium circulating in the channel) but without BL21 transmitting cells in the channel. While the fluorescence-intensity plot in Figure 7f indicates a linear increase of the RFP production of the entrapped cells as the culturing time increased, the negative control showed almost no changes. This

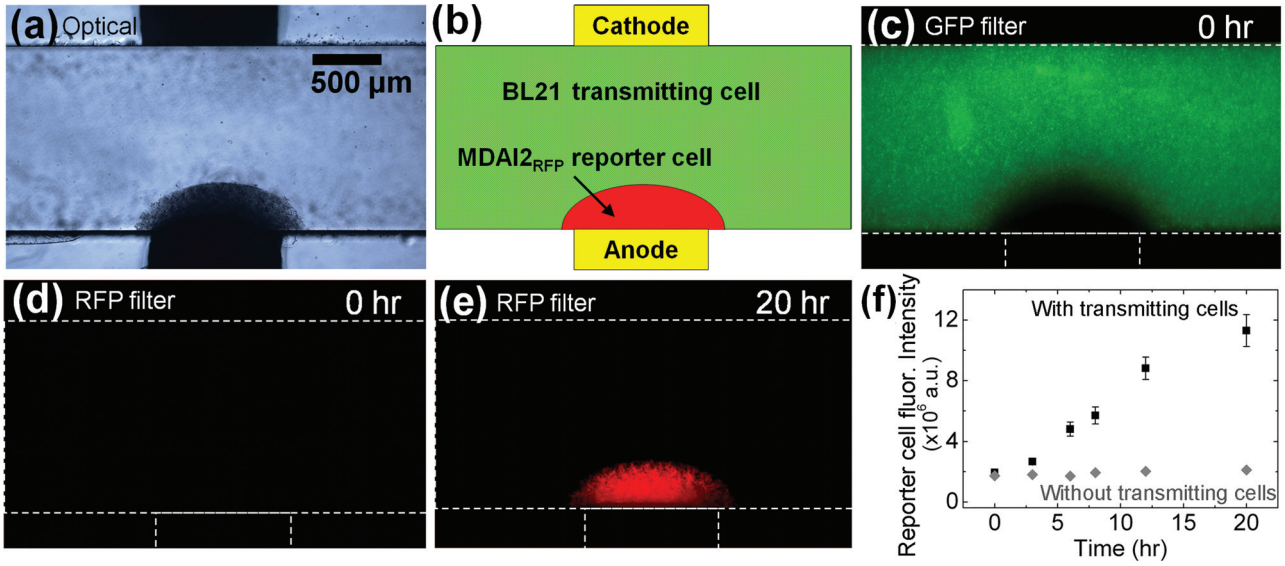

Figure 7. Signaling between a transmitting cell suspended externally and the alginate-entrapped reporter-cell population. a) Bright-field optical image showing the co-deposition of MDAI2$_{RFP}$ reporter cells with calcium alginate gel. b) Schematic diagram of the experimental set-up and configuration. MDAI2$_{RFP}$ reporter cells were immobilized within the gel on the electrode and the channel was filled with BL21 transmitting cells. c–d) Fluorescence images of the channel at time = 0 h with the GFP (c) and RFP (d) filter sets. e) Fluorescence image of the channel at time = 20 h using only the RFP filter set, where a significant amount of fluorescence can be seen inside the gel. f) Plot of the fluorescence intensity of the gel as a function of the coculturing time. The grey dots represent a control sample without a transmitting-cell suspension present in the channel.

clearly demonstrates small-molecule signaling between the gel-entrapped reporter bacterial population and the liquid-phase transmitting population, using our assembly technique and the fluidic biological micro-electromechanical system (bioMEMS). One possible limitation of our electroaddressable model biofilm is a bacterial outgrowing problem for long-term culturing. Within 1 d, the growth and proliferation of bacterial cells still remains within the gel; beyond 1 d, due to the exponential growth of bacterial population, we start to see clumps of colonies growing on the microfluidc channel wall due to chemotaxis driving the cells to seek nutrients outside of the gel.

3. Conclusions

We report a functional, hydrogel-forming calcium alginate composite material with the capability of quantitatively and spatiotemporally creating a model bacterial biofilm entrapping bacterial cells, with 3D control using electrical signals. This material is unique because the in situ cell entrapment can be electrically controlled, which allows control of the bacterial population density and distribution. The demonstrated in situ cell entrapment in an arbitrary and array electrode geometry, with spatial resolution down to tens of micrometers, provides a promising platform for selective and electroaddressable cell patterning and culturing on a 2D surface. The fact that the cell assembly can be quantitatively controlled using this method allows us to study the population-dependent multicellular behavior in a controlled fashion using mimetic bacterial biofilms. The reported multistrain cell coassembly and stratified cell assembly with controlled separation in pseudo-3D hydrogel structures expands our toolbox towards understanding the distance-dependent interactions and communication between the same or different species of cell colonies. The induced protein expression and quorum-sensing behavior of the bacterial cells entrapped in the pseudo-3D model biofilms, demonstrated in our microfluidic device, exemplify the capability of this material for cell culture and cell-cell signaling studies.

These results are significant in providing a versatile approach for assembling model bacterial biofilms at desired locations with a well-defined spatial extent in a microenvironment. The bioMEMS device in use exemplifies an exceptional observation platform that enables microscopic accessibility for biological investigation and the study of bacterial biofilms. These critical features allow us to access the key aspects of bacterial behavior, from metabolic pathways for signal-molecule synthesis to signal-mediated intra- and intercellular cross-talk.

4. Experimental Section

Device Fabrication: The planar 2D chips were fabricated with thermally evaporated chromium and gold on glass slides. Photolithography was performed to define the 5 × 5 arrays of the circular electrode patterns. Electrical passivation on the electrode contact leads was defined via the coating of insulating materials and additional photolithography. The fabrication details of the planar devices with a 5 × 5 electrode array and the UMD logo are described in the supporting information (Figure S4 and S5).

The microfludic device with built-in sidewall electrodes was fabricated by angled thermal evaporation of chromium and gold through a bent stainless-steel shadow mask with 1 mm-wide slits (Figure 1a). Two patterned glass slides with parallel electrodes defined on the sidewall and the top of the glass were placed side by side (separation = 1 mm) sandwiched by two pieces of PDMS layers to form the fluidic channel (cross section = 1 mm × 1 mm). The details of the fabrication of the microfluidic device are described in the supporting information (Figure S6). One limitation of our microfluidic device is the degradation of the electrodes after long-term, multiple electrodeposition runs at high electric-current density. As the top gold layer remains stable and intact during anodic electrochemical reactions, the chromium layer underneath partially reacts with electrochemically generated hydronium ions and causes the electrode degradation.

Alginate-Solution Preparation: 1% and 2% (w/v) sodium alginate solutions were prepared by dissolving sodium alginate powder (Sigma–Aldrich, extracted from brown algae, medium viscosity) in distilled water, followed by ultrasonication (10 min) and stirring (10 h). Sodium alginate deposition solutions with different $CaCO_3$ concentrations (w/v, 0.25%, and 0.5%) were prepared by suspending different amounts of $CaCO_3$ powder (Sigma–Aldrich) into the sodium alginate solutions with constant stirring. To assist visualization and examine the uniformity of the electrodeposited hydrogel, amine-modified fluorescent microspheres (1 μm diameter) (Invitrogen, F8765) were used to fluorescently label the alginate through amine-carboxylate interactions. 2 μl of the fluorosphere solution was added to 2 ml of the alginate solution (0.25% $CaCO_3$, 1% alginate) followed by 1 min vortexing for an even distribution of the microspheres.

Sodium chloride, sodium citrate and calcium chloride solutions (Sigma–Aldrich) were prepared at a 10×10^{-3} M concentration to rinse, dissolve and reinforce the calcium alginate hydrogel, respectively.

Cell-Solution Preparation: Several *E. coli* strains were used in this study. The *E. coli* strain that expresses DsRed was used for the quantitative assembly; we have called it "red *E. coli*" for short. In the first set of experiments, the red *E. coli* with an OD (measured at a wavelength of 600 nm) of 12 (where 1 OD ≈ 1×10^9 cells ml^{-1}) were diluted to a series of concentrations (12, 9, 6, 3, 1.2, and 0.6) and were separately mixed with the alginate solutions for electrodeposition at a constant current density and constant deposition time. In the second set of experiments, red *E. coli* with an OD of around 4 were mixed with the alginate solution and electrodeposited at a constant current density but for different durations of deposition time.

E. coli strains that express DsRed, GFP and BFP (with an OD between 6 and 8) were used to demonstrate their sequential, site-specific, discrete assembly and multilayer assembly with the electrodeposition of calcium alginate hydrogel by seperately mixing different strains of cells with alginate solutions. LB medium with kanamycin (50 μg ml^{-1}) were used to prepare the red and the green *E. coli*, and LB medium with ampicillin (50 μg ml^{-1}) was used for the blue *E coli* to prevent contamination.

Induction and Signaling Sample Preparation: The *E. coli* strain BL21(DE3) (pET-BFP), capable of expressing BFP, was used to characterize the cellular response to IPTG induction. This strain was assembled in the calcium alginate hydrogel and cultured in LB medium containing 1×10^{-3} M IPTG with a flow rate of 2 μl min^{-1}. Ampicillin was added to the LB medium at a concentration of 50 μg ml^{-1} to prevent contamination and 1×10^{-3} M $CaCl_2$ was included to maintain the gel integrity. The control experiment was carried out under the same conditions but without IPTG. The fluorescence intensity of the induced cells was measured as a function of induction time.

E. coli strains that had altered abilities to recognize and respond to autoinducer-2 (AI-2) were used to evaluate cell-cell signaling. Briefly, *E. coli* MDAI2 (pCT6 + pET-DsRed) is a *Lux*S knockout strain that is unable to synthesize AI-2 but can respond to exogenous AI-2 and trigger the expression of DsRed, and therefore plays the role of the reporter cell. The transmitting cell, BL21 (pCT5 + pET-GFP) is an *E. coli* strain that can generate AI-2 and constitutively express GFP. The signaling experiment was performed by firstly depositing the reporter cells (with an OD ≈ 2) using cell-alginate-$CaCO_3$ deposition solution onto a specific electrode

address. Then, the fluidic channel was filled with transmitting cells (with an OD ≈ 12) in LB medium with $CaCl_2$ (1×10^{-3} M), ampicillin (50 μg ml^{-1}) and kanamycin (50 μg ml^{-1}). The transmitting-cell solution was flowed back and forth over the hydrogel region containing the reporter cells, MDAI2 (pCT6 + pET-dsRed) by a pulsed pushing and pulling of the syringe pump (2 μl min^{-1}, switching flow direction every 1 h). The fluorescent signal of the assembled reporter cells was monitored as a function of culturing time.

Bright-Field and Fluorescence Imaging: Bright-field optical microscopy and fluorescence microscopy were performed using a Zeiss LSM-310 laser-scanning confocal microscope. The bright-field optical-microscopy images were obtained with transmitted incandescent light from below. The fluorescence-microscopy images for *E. coli* expressing DsRed, GFP and BFP were obtained using TRITC, GFP and BFP filter sets.

Supporting Information

Supporting Information is available from the Wiley Online Library or from the author.

Acknowledgements

We acknowledge the Maryland NanoCenter and its FabLab for the device fabrication. This work was supported by the Robert W. Deutsch Foundation, US Navy ONR N000141010446, and NSF-EFRI NSF-SC03524414.

Received: August 20, 2011
Revised: September 30, 2011
Published online: November 29, 2011

[1] C. A. Arias, B. E. Murray, *New England J. Medicine* **2009**, *360*, 439.
[2] H. C. Neu, *Science* **1992**, *257*, 1064.
[3] M. C. Enright, D. A. Robinson, G. Randle, E. J. Feil, H. Grundmann, B. G. Spratt, *Proc. Natl. Acad. Sci. USA* **2002**, *99*, 7687.
[4] L. Hall-Stoodley, J. W. Costerton, P. Stoodley, *Nature Rev. Microbiol.* **2004**, *2*, 95.
[5] T.-F. C. Mah, G. A. O'Toole, *Trends Microbiol.* **2001**, *9*, 34.
[6] E. Drenkard, F. M. Ausubel, *Nature* **2002**, *416*, 740.
[7] D. T. Hung, E. A. Shakhnovich, E. Pierson, J. J. Mekalanos, *Science* **2005**, *310*, 670.
[8] D. A. Rasko, C. G. Moreira, D. R. Li, N. C. Reading, J. M. Ritchie, M. K. Waldor, N. Williams, R. Taussig, S. Wei, M. Roth, D. T. Hughes, J. F. Huntley, M. W. Fina, J. R. Falck, V. Sperandio, *Science* **2008**, *321*, 1078.
[9] G. C. L. Wong, G. A. O'Toole, *MRS Bull.* **2011**, *36*, 339.
[10] W. S. Choi, D. Ha, S. Park, T. Kim, *Biomaterials* **2011**, *32*, 2500.
[11] B. Xie, R. L. Parkhill, W. L. Warren, J. E. Smay, *Adv. Funct. Mater.* **2006**, *16*, 1685.
[12] D. W. Green, I. Leveque, D. Walsh, D. Howard, X. Yang, K. Partridge, S. Mann, R. O. C. Oreffo, *Adv. Funct. Mater.* **2005**, *15*, 917.
[13] H. L. Lim, J. C. Chuang, T. Tran, A. Aung, G. Arya, S. Varghese, *Adv. Funct. Mater.* *21*, 55.
[14] C. M. Nelson, J. Tien, *Curr. Opin. Biotechnol.* **2006**, *17*, 518.
[15] C. M. Nelson, M. M. VanDuijn, J. L. Inman, D. A. Fletcher, M. J. Bissell, *Science* **2006**, *314*, 298.
[16] A. Khademhosseini, R. Langer, J. Borenstein, J. P. Vacanti, *Proc. Natl. Acad. Sci. USA* **2006**, *103*, 2480.
[17] Y. Luo, M. S. Shoichet, *Nat. Mater.* **2004**, *3*, 249.
[18] M. W. Tibbitt, K. S. Anseth, *Biotechnol. Bioeng.* **2009**, *103*, 655.
[19] B. M. Gillette, J. A. Jensen, B. X. Tang, G. J. Yang, A. Bazargan-Lari, M. Zhong, S. K. Sia, *Nat. Mater.* **2008**, *7*, 636.
[20] P. Zorlutuna, J. H. Jeong, H. Kong, R. Bashir, *Adv. Funct. Mater.* **2011**, *21*, 3642.
[21] A. Boyd, A. M. Chakrabarty, *J. Ind. Microbiol. Biotechnol.* **1995**, *15*, 162.
[22] H.-C. Flemming, J. Wingender, *Nature Rev. Microbiol.* **2010**, *8*, 623.
[23] X. W. Shi, C. Y. Tsao, X. Yang, Y. Liu, P. Dykstra, G. W. Rubloff, R. Ghodssi, W. E. Bentley, G. F. Payne, *Adv. Funct. Mater.* **2009**, *19*, 2074.
[24] Y. Cheng, X. Luo, J. Betz, G. F. Payne, W. E. Bentley, G. W. Rubloff, *Soft Matter* **2011**, *7*, 5677.
[25] L.-Q. Wu, A. P. Gadre, H. Yi, M. J. Kastantin, G. W. Rubloff, W. E. Bentley, G. F. Payne, R. Ghodssi, *Langmuir* **2002**, *18*, 8620.
[26] X.-L. Luo, J.-J. Xu, Y. Du, H.-Y. Chen, *Anal. Biochem.* **2004**, *334*, 284.
[27] X. Pang, I. Zhitomirsky, *Mater. Chem. Phys.* **2005**, *94*, 245.
[28] M. Cheong, I. Zhitomirsky, *Colloids Surf. A: Physicochem. Eng. Aspects* **2008**, *328*, 73.
[29] Y. Cheng, X. Luo, J. Betz, S. Buckhout-White, O. Bekdash, G. F. Payne, W. E. Bentley, G. W. Rubloff, *Soft Matter* **2010**, *6*, 3177.
[30] Y. Cheng, X. Luo, C.-Y. Tsao, H.-C. Wu, J. Betz, G. F. Payne, W. E. Bentley, G. W. Rubloff, *Lab Chip* **2011**, *11*, 2316.
[31] R. Fernandes, L.-Q. Wu, T. Chen, H. Yi, G. W. Rubloff, R. Ghodssi, W. E. Bentley, G. F. Payne, *Langmuir* **2003**, *19*, 4058.
[32] O. Smidsrød, G. Skjåk-Braek, *Trends Biotechnol.* **1990**, *8*, 71.
[33] J. A. Rowley, G. Madlambayan, D. J. Mooney, *Biomaterials* **1999**, *20*, 45.
[34] C. Y. Tsao, S. Hooshangi, H. C. Wu, J. J. Valdes, W. E. Bentley, *Metabolic Eng.* **2010**, *12*, 291.
[35] C. A. Fux, J. W. Costerton, P. S. Stewart, P. Stoodley, *Trends Microbiol.* **2005**, *13*, 34.
[36] P. S. Stewart, J. William Costerton, *Lancet* **2001**, *358*, 135.
[37] M. B. Miller, B. L. Bassler, *Annu. Rev. Microbiol.* **2001**, *55*, 165.
[38] C. D. Nadell, J. B. Xavier, K. R. Foster, *FEMS Microbiol. Rev.* **2009**, *33*, 206.
[39] W. C. Fuqua, S. C. Winans, E. P. Greenberg, *J. Bacteriology* **1994**, *176*, 269.
[40] C. M. Waters, B. L. Bassler, *Annu. Rev. Cell Developmental Biol.* **2005**, *21*, 319.
[41] M. G. Surette, M. B. Miller, B. L. Bassler, *Proc. Natl. Acad. Sci.* **1999**, *96*, 1639.
[42] J. D. Shrout, T. Tolker-Nielsen, M. Givskov, M. R. Parsek, *MRS Bull.* **2011**, *36*, 367.